Neurochemical Research (2022) 47:148–162
https://doi.org/10.1007/s11064-021-03247-8

ORIGINAL PAPER

Pre-Steady-State Kinetics and Reverse Transport in Rat Glutamate Transporter EAAC1 with an Immobilized Transport Domain

Jiali Wang[1] · Laura Zielewicz[1] · Yang Dong[1] · Christof Grewer[1]

Received: 4 November 2020 / Revised: 15 January 2021 / Accepted: 18 January 2021 / Published online: 6 February 2021

Abstract

Plasma membrane glutamate transporters move glutamate across the cell membrane in a process that is thought to involve elevator-like movement of the transport domain relative to the static trimerization domain. Conformational changes associated with this elevator-like movement have been blocked by covalent crosslinking of cysteine pairs inserted strategically in several positions in the transporter structure, resulting in inhibition of steady-state transport activity. However, it is not known how these crosslinking restraints affect other partial reactions of the transporter that were identified based on pre-steady-state kinetic analysis. Here, we re-examine two different introduced cysteine pairs in the rat glutamate transporter EAAC1 recombinantely expressed in HEK293 cells, W440C/K268C and K64C/V419C, with respect to the molecular mechanism of their impairment of transporter function. Pre-steady-state kinetic studies of glutamate-induced partial reactions were performed using laser photolysis of caged glutamate to achieve sub-millisecond time resolution. Crosslinking of both cysteine pairs abolished steady-state transport current, as well as the majority of pre-steady-state glutamate-induced charge movements, in both forward and reverse transport mode, suggesting that it is not only the elevator-like movement associated with translocation, but also other transporter partial reactions that are inhibited. In contrast, sodium binding to the empty transporter, and glutamate-induced anion conductance were still intact after the W440C/K268C crosslink. Our results add to the previous mechanistic view of how covalent restraints of the transporter affect function and structural changes linked to individual steps in the transport cycle.

Keywords Glutamate transporter · Crosslink · Electrophysiology · Kinetics · Laser-photolysis

Introduction

Plasma membrane glutamate transporters are responsible for transporting the major excitatory neurotransmitter, glutamate, across cell membranes [1–3]. Glutamate transporters take up glutamate into the cell against the glutamate concentration gradient, by co-transporting three sodium ions and one proton, and counter-transporting a potassium ion [1, 3–7]. The stoichiometry of transport is 3:1:1:1 (Na^+:Glu-:H^+:K^+), resulting in the net movement of two positive charges into the cell for each transported glutamate molecule [1, 4, 8, 9]. During the translocation process, glutamate transporters also catalyze uncoupled anion currents that are proportional to glutamate transport activity [4, 10–14].

The structure of glutamate transporters was first studied using the archaeal homologue Glt_{ph}, which shares 37% sequence identity and 55% similarity with human transporter subtype hEAAT2, excitatory amino acid transporter 2 [15]. The transporter is assembled as a homotrimer with three identical subunits working independently of each other [16–18]. Two major conformations (outward-facing and inward-facing states, OFS/IFS) of the glutamate transporter were discovered for Glt_{ph} and resolved using x-ray crystallography [19, 20]. The inward-facing state was also identified by the Kanner group on the basis of structural modeling of inverted sequence repeats [21]. The generally-accepted molecular mechanism of glutamate transport is predicted to be based on successive steps, including extracellular substrate binding, translocation, and release to the cytosol [22, 23]. The translocation steps are associated with

Special Issue: In Honor of Prof. Baruch Kanner.

✉ Christof Grewer
cgrewer@binghamton.edu

[1] Department of Chemistry, Binghamton University, 4400 Vestal Parkway East, Binghamton, NY 13902, USA

conformational changes of the transport domain, which functions in an elevator-based alternating access mechanism [24]. The trimerization domain, on the other hand, is thought to function as a static scaffold for the dynamic transport domain.

Transporter crosslinking studies, to restrict the transporter chemically to certain conformations, have been performed by several research groups [20, 21, 25]. By crosslinking the trimerization and transport domain between transmembrane domains TM5 and TM8, glutamate uptake was inhibited, likely by blocking the substrate translocation process. In addition, crosslinking was performed to stabilize the inward-facing conformation of Glt_{Ph} for structure determination. For the present crosslinking study, we chose to introduce disulfide bridges in two major conformations, inward-facing (IFS) and outward-facing (OFS) states. The inward-facing conformation was proposed to be stabilized by the crosslinked K55C/V364C double-cysteine mutant transporter, which crosslinks Glt_{ph} between TM2 and HP2 [20, 21]. The outward-facing state was studied using the W440C/K268C pair, located in TM5 and TM8, following the research published by the Kanner group [25].

Here we use the laser-pulse photolysis method to perform rapid kinetic studies on glutamate transporters with the crosslinks described above. The results from these kinetic studies were compared with results from rapid solution exchange experiments at steady state. Laser-pulse photolysis experiments were performed with the glutamate transporter previously [26, 27], in which caged glutamate was applied to cells, followed by photolysis of caged glutamate initiated with a nanosecond laser pulse. Rapid transient current signals were recorded on a millisecond time scale, providing information about early steps in the transport cycle, such as glutamate and sodium binding. Here we applied the laser-photolysis method to glutamate transporters with known crosslinks to the transport domain, to analyze their kinetic behavior on a short time scale. Notably, the crosslinks abolish pre-steady state currents previously assigned to glutamate translocation and other pre-steady-state current components closely linked to it. However, Na^+ binding to the empty transporter does not appear to be affected by the crosslinks, suggesting that it does not require large-scale conformational changes of the transport domain.

Results

Positions of Paired Cysteine Mutagenesis in EAAC1

Paired cysteine mutagenesis experiments were conducted using the rat glutamate transporter EAAC1 (excitatory amino acid carrier 1), in order to restrict movement of transporter domains relative to each other through covalent crosslinking, for example the transport domain relative to the trimerization domain, followed by rapid kinetic studies of transporter function. Positions were selected based on the Glt_{ph} structure and inspired by recent publications performing crosslinking in the human EAAC1 analog, EAAT3, and Glt_{Ph} [19–21, 25] (Fig. 1a–c). We constructed two double-cysteine mutants to positions in the transport domain and trimerization domain, W440C/K268C, in TM5 and TM8, and K64C/V419C, in TM2 and HP2. The K64C/V419C mutations were based on conserved residues located in Glt_{ph}, which, through cadmium complexation or the formation of a disulfide bond, crosslink the transporter into the inward-facing conformation [20] (Fig. 1c). The two introduced cysteine residues, located within TM2 and HP2 domains, are predicted to be 3.76 Å apart in the inward-facing conformation (Fig. 1c), while the distance is 21.6 Å in the outward-facing conformation (Fig. 1a), and 14.7 Å in the intermediate state (Fig. 1b). Another double-cysteine mutant, W440C/K268C, was chosen following the research published by the Kanner group [25]. After crosslinking, the W440C/K268C glutamate transporter is predicted to be restricted to sampling the outward-facing state and intermediate state, with distances ranging from 3.5 to 7.3 Å between the two residues (Fig. 1a, b). However, the cysteine pair's distance increased to 14.9 Å when the transport domain was in the inward-facing conformation. From previous results, these two double-cysteine mutants were predicted to be close enough to form disulfide bonds under oxidizing conditions. In previous results, preincubation of HELA cells expressing W440C/K268C double mutant with 1 µM CuPh or $CdCl_2$ resulted in an inhibition of D-[^{3}H]aspartate transport by 60–70%, and over 95% inhibition when using 8 µM crosslinking reagent [25].

Crosslinking Results in Inhibition of Steady-State Anion Currents

We first tested the activity of the $EAAC1_{cysless}$ transporter and the two double-cysteine mutant transporters described in the last paragraph, before and after crosslinking. These experiments were performed in the presence of extracellular Na^+/glutamate and intracellular K^+, i.e. the forward transport mode, in which the amino acid substrate is transported across the membrane to the intracellular side. Anion current was observed upon application of glutamate to $EAAC1_{cysless}$, as shown in Fig. 2a. These currents were inwardly directed due to the outflow of internal SCN^-, caused by the population of an anion conducting state located along the translocation pathway [4, 11, 26, 28]. The glutamate dose response relationship for this current is shown in Fig. 2b with an apparent affinity of $K_m = 13.4 \pm 2.5$ µM, a value that is only slightly larger than that of the wild type transporter (Fig. 2e). These results show that the cysless transporter

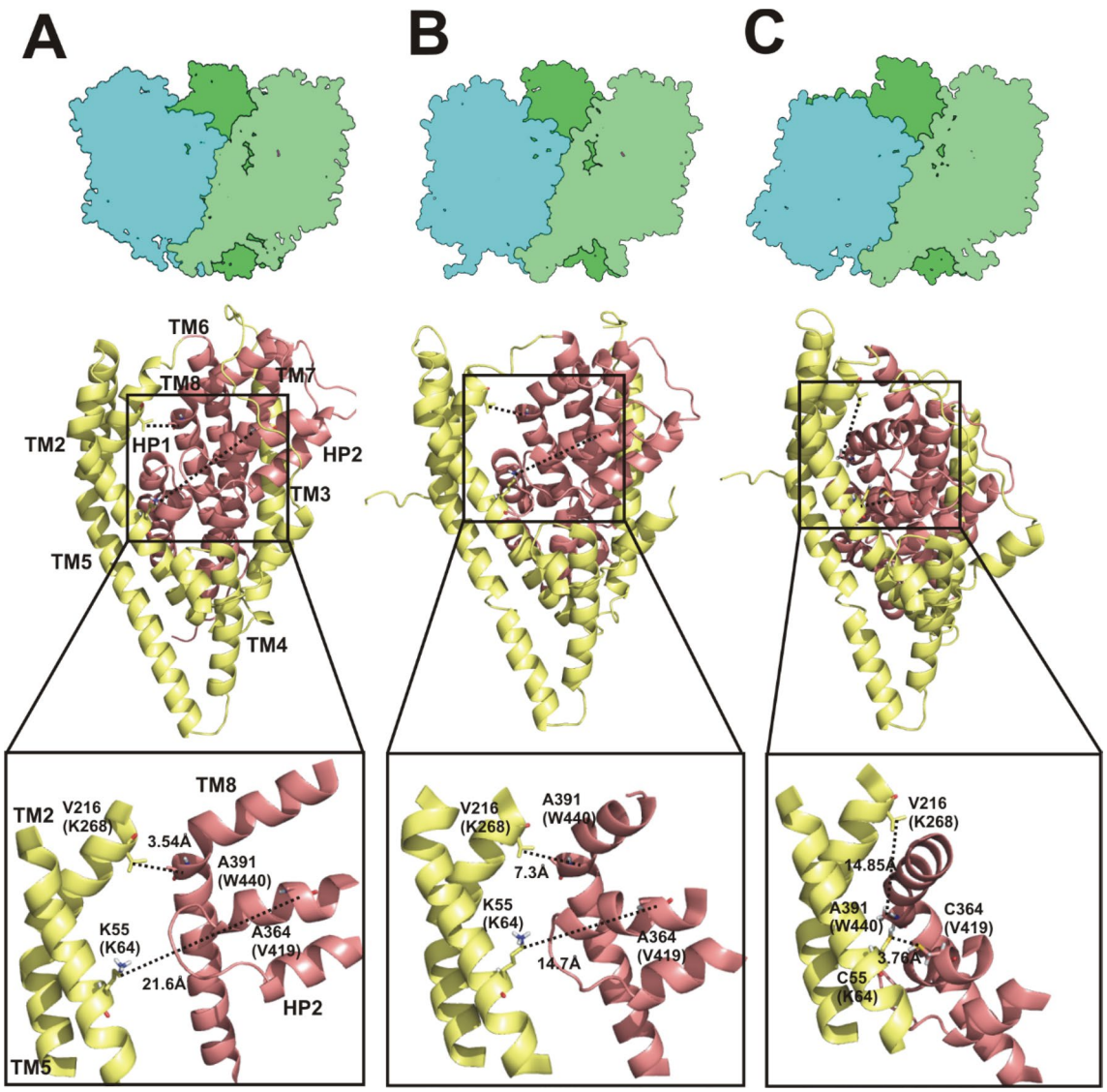

Fig. 1 Predicted locations of the introduced cysteine pairs in homologue structure Glt_{ph} in three different conformations. The upper panel shows cartoon representation of Glt_{ph} structures (PDB IDs:2nwx,3v8g,3kbc) in the outward-facing state (**a**), the outward-facing intermediate state (**b**), and the inward facing state (**c**). Three identical subunits are colored as blue, dark green, and light green. The blue-colored subunit (left), illustrates the conformational change. The lower panels illustrate the transport domain in pink and the trimerization domain in yellow. The mutated residues are highlighted and labeled. Distances were calculated based on atom K64(CE), V419(CA), K268(CB), W440(CA) and are labeled in ångstroms. All images were generated using PyMOL software. The amino acids in parentheses represent EAAT3 numbering

is functional with kinetic properties close to the wild type transporter. The two double-cysteine-mutant transporters were also active (dose response curves shown in Fig. 2c and d), although with slightly smaller glutamate-induced anion currents compared to $EAAC1_{cysless}$ (Fig. 2f). However, this reduction in current was not statistically significant. The apparent K_m values for glutamate of the two mutant transporters are shown in Fig. 2c, with only a minor difference in apparent glutamate affinity between $EAAC1_{WT}$ (8.1 ± 1.5 µM), $EAAC1_{Cysless}$ (13.4 ± 2.5 µM), $EAAC1_{K64C/V419C}$ (16.3 ± 3.0 µM), and $EAAC1_{K268C/W440C}$ (25.6 ± 4.0 µM), summarized in Fig. 2e.

As demonstrated in previous studies, crosslinking of two cysteine residues in glutamate transporters can be achieved by either Cd^{2+} or copper phenanthroline (CuPh) application [25]. In order to observe the full inhibition effect, we applied 400 µM CuPh, a higher value compared to the previous studies [25], with or without 400 µM $CdCl_2$ in the pipette (intracellular side application) with similar results. An incubation time of 15 min with external 400/400 µM $CuPh/CdCl_2$ resulted in an inhibition of glutamate-induced

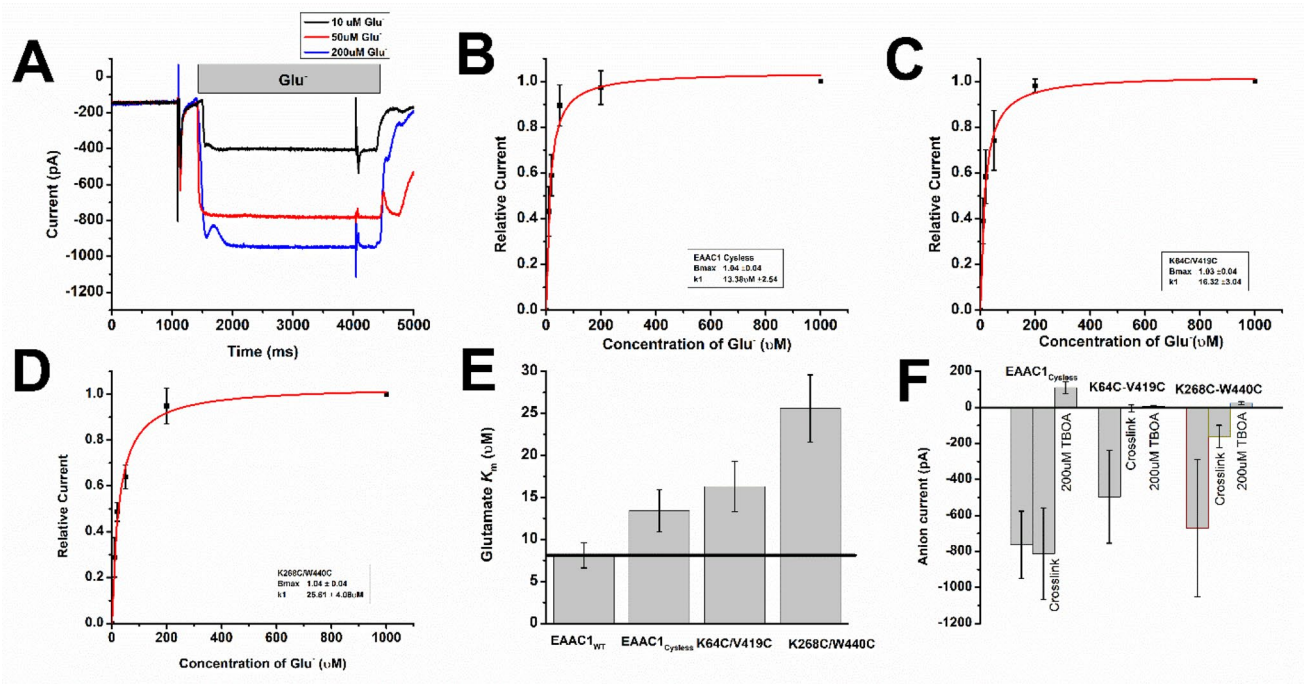

Fig. 2 Double-cysteine mutations block the anion conductance under oxidizing conditions. Whole-cell current recording experiments with $EAAC1_{Cysless}$ were performed under ionic conditions favoring the observation of the anion conductance, using the permeant anion SCN^-: 130 mM KSCN in the pipette solution,140 mM NaMes in the extracellular solution. Extracellular glutamate was applied at the time indicated by the grey bar at V = 0 mV. **a**) Typical anion current recordings induced by 10/50/200 µM glutamate. **b**, **c**, **d** Dose response curve to determine the $EAAC1_{Cysless}$, $EAAC1_{K64C/V419C}$ and $EAAC1_{K268C/W440C}$ glutamate apparent affinities. The solid line is a fit to a Michaelis–Menten-like equation. **(E)** Glutamate K_m values for wild-type and mutant transporters before crosslinking: $EAAC1_{wt}$ $K_m = 8.1 \pm 1.5$ µM (n = 18), $EAAC1_{Cysless}$ $K_m = 13.4 \pm 2.5$ µM (n = 17), $EAAC1_{K64C/V419C}$.$K_m = 16.3 \pm 3.0$ µM (n = 9) and $EAAC1_{K268C/W440C}$ $K_m = 25.6 \pm 4$ µM (n = 12). **f** Maximum anion currents (at saturating glutamate concentration) under forward transport conditions before and after crosslinking. Crosslink reagents were used at the concentration of 400 µM/400 µM CuPh and $CdCl_2$ from extracellular and intracellular side, respectively. Student's t-test analysis indicated the crosslink effects were significant for K268C/W440C, $p < 0.00001$, and for K64C/V419C, $p < 0.0000001$. For all experiments in the presence of TBOA, the inhibitor was added after crosslinking

anion current activity by 74% for $EAAC1_{K268C/W440C}$ and over 95% for $EAAC1_{K64C/V419C}$ (Fig. 2d), respectively. Therefore, $EAAC1_{K64C/V419C}$ showed a slightly more pronounced crosslinking effect on the current. Moreover, cells expressing $EAAC1_{cysless}$ were also tested as a control using the same concentration of crosslinking reagent and showed no inhibition effect (Fig. 2d). We also tested the effect of crosslinking on the leak anion conductance. DL-TBOA (DL-*threo*-beta-benzyloxyaspartate), a high affinity glutamate transporter inhibitor was used to block the leak anion conductance. The results shown in Fig. 2d demonstrate that Na^+-induced leak anion currents were inhibited by crosslinking of both double mutant transporters, as evidenced by the lack of outward current upon application of TBOA. In contrast, TBOA induced outward current in $EAAC1_{cysless}$ due to outflow of SCN^- being blocked by TBOA (Fig. 2d). While these data do not fully exclude the possibility that TBOA does not bind to the transporters after crosslinking, this explanation is less likely because glutamate can still bind to the crosslinked transporter, and TBOA can block Na^+-induced transient currents in voltage jump experiments (see below).

We also determined the voltage dependence of the currents to test the crosslink effect. Under ionic condition favoring the forward transport mode, and with SCN^- in the pipette, currents before crosslinking were increased by negative transmembrane potential, as expected for glutamate induced anion current caused by SCN^- outflow (Fig. 3a and c). Current–voltage relationships (I-V curves) are shown in Fig. 3b and d. Currents were strongly inhibited after crosslinking for both double mutant transporters, although the effect was more complete for $EAAC1_{K64C/V419C}$. Background currents were subtracted by application of 400 µM TBOA. We attempted to reverse the crosslinking effect by using DTT after current recording in the crosslinked state, with limited success. The reason is that it is more difficult to do long term experiments in patch-clamped cells, as compared to other experimental methods, due to the cells having a limited lifetime when attached to the pipette in the whole-cell recording mode.

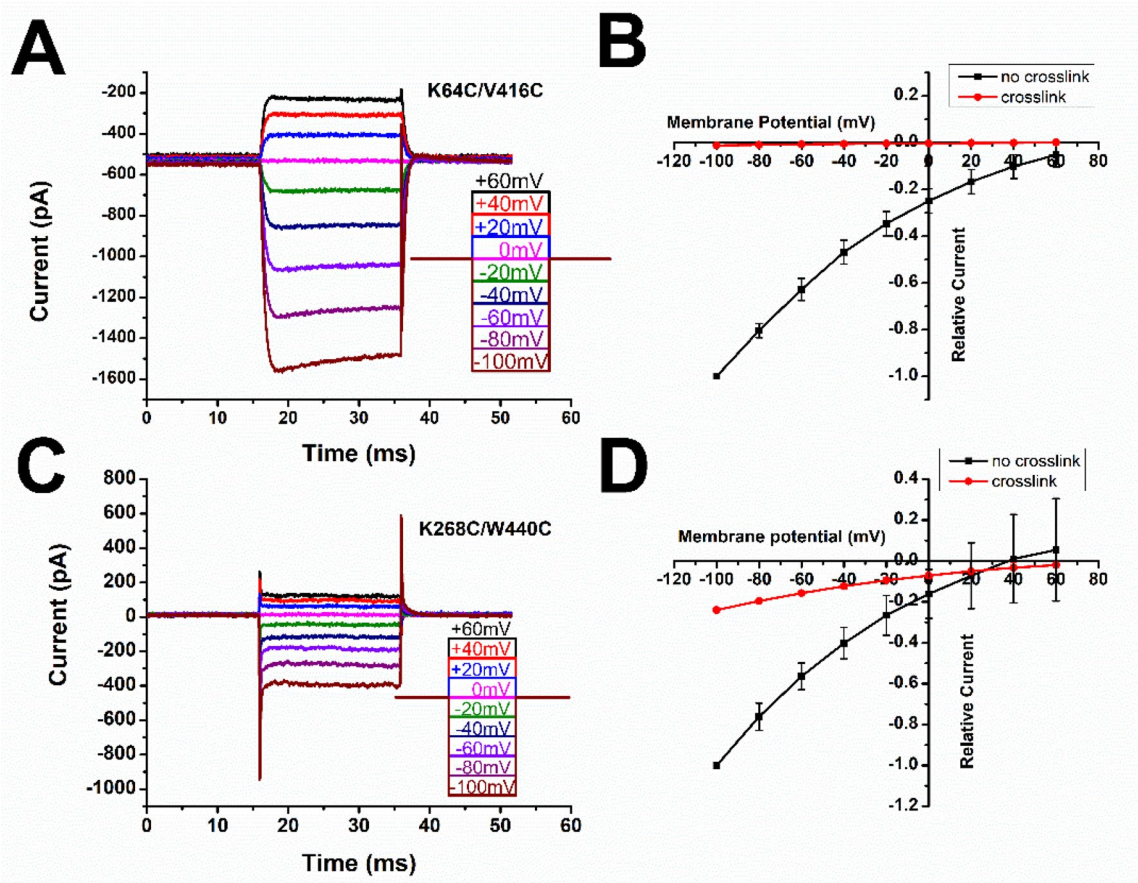

Fig. 3 Glutamate-induced anion current is inhibited by crosslinking of double-mutant transporters. **a** and **c** Voltage-dependent $EAAC1_{K64C/V419C}$ and $EAAC1_{K268C/W440C}$ anion currents were activated by extracellular application of 1 mM glutamate in the presence of the intracellular permeant anion SCN^-. The extracellular solution contained 140 mM NaMES, the intracellular solution contained 130 mM KSCN, forward transport conditions. The voltage jump protocol is show as inset (see *Materials and Methods*). The membrane potential range was -100 mV to + 60 mV. **b** and **d** $EAAC1_{K64C/V419C}$ and $EAAC1_{K268C/W440C}$ anion current–voltage relationship at steady state before (black, n = 7 and 11) and after crosslinking (red, n = 17 and 15). Background currents were obtained by application of 200 µM TBOA and subtraction

Pre-Steady-State Currents in the Forward Transport Mode are Inhibited in the Crosslinked State

EAAC1 pre-steady-state currents, in response to rapid application of glutamate, have been described previously [26, 27, 29]. These currents provide important information about early steps in the glutamate transport cycle. Therefore, we measured glutamate-induced pre-steady-state currents in the crosslinked transporters, to test which reaction steps are affected by the covalent modification. The time course of pre-steady-state kinetics of EAAC1 currents was recorded using ionic conditions that favor observation of the transport current, i.e. inside K^+, outside Na^+ and replacement of Cl^- by the non-permeant methansulfonate ion [26, 29]. In the cysless mutant transporter, a glutamate concentration jump induced by laser-pulse photolysis of caged glutamate resulted in a large, inwardly-directed transient current (Fig. 4a), which decayed to a steady state with two-exponential behavior, as described previously for the EAAC1 wild-type transporter [26, 29], and for other EAATs using fast solution exchange methods [28, 30–32]. The transient current fully decayed to the steady state within 25 ms, in analogy to previous results with wild-type EAAC1, indicating that the pre-steady-state kinetics are not dramatically affected by introducing the five Cys to Ser mutations.

After introducing the double mutants in the cysless background, both pre-steady-state and steady-state currents under forward transport conditions were reduced in K64C/V419C and K268C/W440C mutant transporters before crosslinking, with the K268C/W440C transporters showing a more significant reduction in currents (Fig. 4b and c). This reduction could be caused by reduced expression levels of the double mutant transporters, slowed kinetics and turnover rate, or disulfide bridge formation before CuPh application. In fact, the latter was shown to be the case for the partial reduction of the current in the K268C/W440C mutant

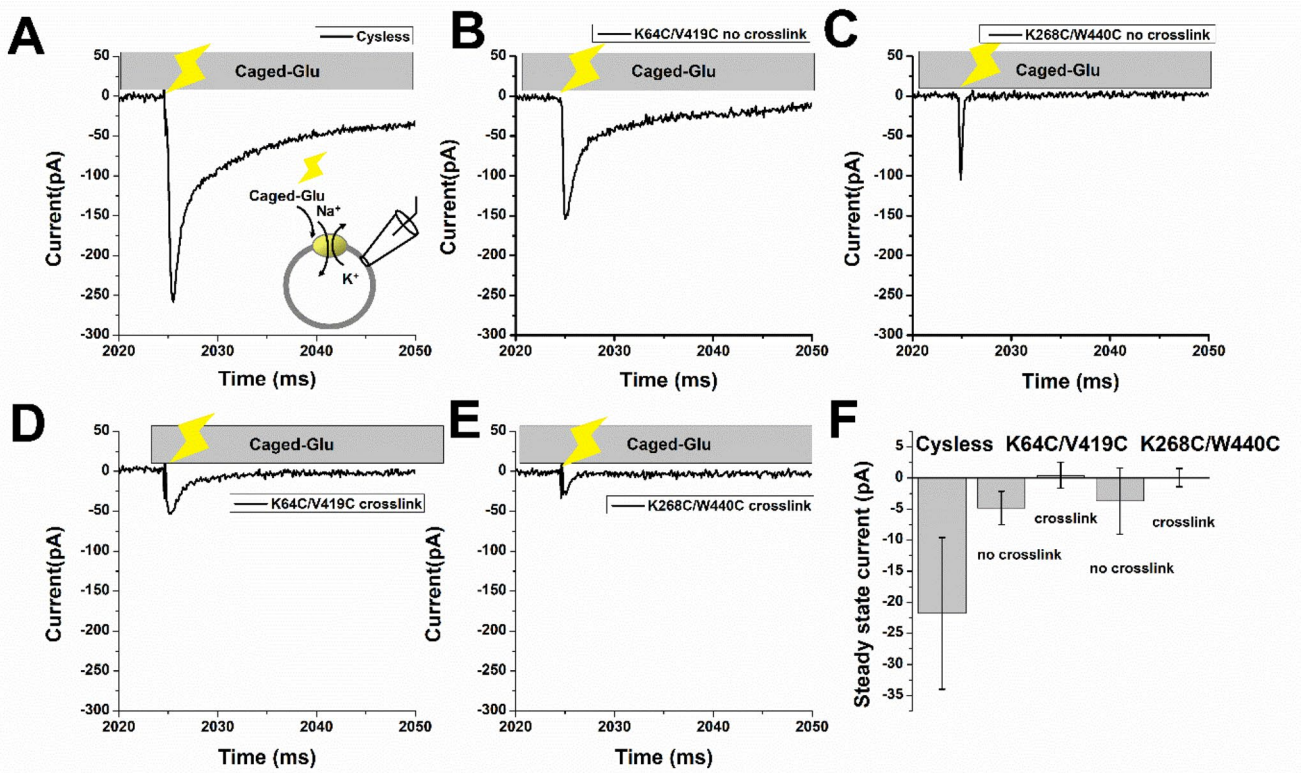

Fig. 4 Crosslinking reduces glutamate-induced transient charge movement under forward-transport conditions. **a** Current recording after photolytic liberation of glutamate from 1 mM MNI-caged glutamate at the time indicated by the flash symbol in $EAAC1_{Cysless}$-expressing HEK293 cells. Photolysis was initiated with a 355 nm laser flash (400 mJ/cm^2). Pre-steady-state currents were measured under forward-transport conditions in the absence of permeant anion, with 140 mM NaMES in the extracellular solution, and 130 mM KMes in the intracellular solution. 1 mM MNI-caged glutamate were pre-equilibrated with the cell for 0.5 s prior to the laser flash. **b** and **c** Similar experiment with $EAAC1_{K64C/V419C}$ and $EAAC1_{K268C/W440C}$ before crosslinking. **d** and **e** Laser photolysis experiment with $EAAC1_{K64C/V419C}$ and $EAAC1_{K268C/W440C}$ after crosslinking. **f** Summary of steady-state current amplitude in response to laser-photolysis of 1 mM caged glutamate. The membrane potential was 0 mV in all experiments. Student's t-test analysis indicated the crosslink effect was significant for K268C/W440C, $p = 0.0002$, and for K64C/V419C, $p < 0.0001$

transporter [25]. To test for expression levels, we performed immunostaining (Suppl. Fig. 1). Immunofluorescence of the double mutant transporters did not appear to be significantly altered compared to the cysless transporter. After crosslinking with CuPh, both pre-steady-state currents (Fig. 4d and e) and steady-state currents (Fig. 4f) were further reduced, as expected by the crosslink immobilizing the transport domain.

While the pre-steady-state currents in $EAAC1_{K268C/W440C}$ could not be quantitatively evaluated before and after crosslinking, due to the small amplitudes, the time constants in $EAAC1_{K64C/V419C}$ of the transient current decay, as well as the amplitude ratio between the two decaying phases were virtually unchanged after crosslinking. This indicates that the crosslink was not 100% complete, and some transporter (< 30%) remained in the active configuration. Despite the inability to fully block transient current by the crosslink in $EAAC1_{K64C/V419C}$, it is clear that all phases of the transient current are severely affected by the immobilization of the transport domain. This is expected for locking the transporter in the inward-facing conformation, in which external glutamate cannot induce the conformational changes triggered by Na^+ binding to the glutamate-bound transporter, and translocation, which were proposed to be responsible for the pre-steady-state charge movement in wild-type EAAC1.

Crosslinks Eliminate EAAC1 Reverse Transport Current and Glutamate Release

K^+-induced relocation of the glutamate-free transporter is an important step in the glutamate transport cycle. Using forward transport conditions, as in the previous paragraphs, intracellular K^+ catalyzes this relocation reaction, to re-expose glutamate binding sites to the extracellular side after translocation is complete. Next, we reversed the ionic gradients across the membrane and used application of extracellular K^+ in the reverse transport mode (in the presence of intracellular Na^+ and glutamate) to test the properties of

mutations together with crosslinking on the relocation steps in the reverse transport direction. In Fig. 5a, a typical steady-state reverse transport current recorded from cells expressing $EAAC1_{cysless}$ is shown. As expected [6, 23, 27, 30, 32, 33], this current is outwardly directed due to the coupled outward movement of two positive charges for each K^+ ion taken up. The outward currents were dependent on the K^+ concentration, as reported previously [30]. The K^+ apparent affinity of $EAAC1_{Cysless}$ was determined as 5.1 ± 1.2 mM, which was in same range as that for $EAAC1_{WT}$ (3.4 ± 0.6 mM) [30].

Next, we performed laser-photolysis experiments, using caged-glutamate inside the recording pipet, to study the rapid kinetics of the reverse translocation process. Here, the extracellular solution contained 140 mM K^+, and the intracellular solution 140 mM Na^+ and 5 mM caged glutamate, which diffused into the cytosol within 5 min after forming the whole-cell mode [27]. As shown previously for the wild-type transporter, outwardly-directed currents were observed upon photolysis in $EAAC1_{cysless}$, as illustrated in Fig. 5c. These currents demonstrated a rapidly decaying outward transient component $\tau = 4.49 \pm 0.84$ ms, which settled to the steady state with a damped oscillation. In contrast, the $EAAC1_{K64C/V419C}$ currents showed a larger initial peak relative to the steady-state current, with slower decay kinetics $\tau = 9.01 \pm 2.34$ ms and no oscillation (Fig. 5d). This indicates that the steady-state turnover rate in the reverse direction is already slowed by the double-mutation before crosslinking, see also Fig. 5h for a summary of steady-state currents. After crosslinking, both steady-state and transient current components were virtually eliminated (Fig. 5f). It was previously proposed that the transient current in the reverse transport direction is caused by the electrogenic reverse translocation process. This assignment is consistent with the data shown in Fig. 5f. In addition, the data indicate that charge movement from partial reaction steps other than translocation may also be impaired by the crosslinking reaction.

For $EAAC1_{K268C/W440C}$ pre-steady-state currents in the reverse transport mode were very small, before and after crosslinking (Fig. 5e and g). This could be caused by the transporter being significantly crosslinked already before CuPh application, as described above. Overall, the data suggest that this double mutation severely impairs any early reactions occurring in the reverse transport reaction after glutamate application, possibly even glutamate binding.

We also studied K^+-driven glutamate efflux to test the mutant transporters' function and crosslink effects using iGluSnFR extracellular glutamate binding sensor [34] (Fig. 6). The fluorescent sensor was co-expressed with rat EAAC1 wild type or mutant DNA in HEK293 cells. We applied varying external K^+ concentrations and measured resulting glutamate release via fluorescence intensity changes. An increase in fluorescence indicates a change from non-bound state to bound state of glutamate to iGluSnFR sensor. First, 10 mM DTT in 140 mM NaMes was used to wash solutions and the original glutamate efflux was measured upon application of 140 mM KMes, by measuring the increase in fluorescence intensity (Fig. 6a). Cells expressing wild type EAAC1 showed a relative fluorescence increase of 1.70 ± 0.06 -fold, and cells expressing the cysless transporter DNA responded similarly (1.55 ± 0.34-fold increase). Both cysteine double-mutant transporters showed much less glutamate efflux under the same conditions (K64C/V419C, 0.39 ± 0.05; K268C/W440C, 0.27 ± 0.08). This data confirms the results from current recordings, namely that the cysteine double-mutant transporters may be less effective at transporting glutamate even before crosslinking. Figure 6b shows the result for the relative change in glutamate efflux for each transporter after crosslinking reagent was applied. The change in glutamate efflux resulting from crosslinking was calculated relative to the original efflux data. Even though the cysteine double-mutants originally showed much less glutamate efflux, they also had a great reduction in efflux as a result of crosslinking, especially when CuPh was used as the crosslinking reagent. $EAAC1_{K64C/V419C}$ and $EAAC1_{K268C/W440C}$ showed only $17.9 \pm 8.5\%$ and $17.4 \pm 11.0\%$ of the original glutamate efflux, respectively, after crosslinking with CuPh. Under the same conditions, the wild type and cysless transporters showed about the same glutamate efflux as they had originally (wild type = $102 \pm 1\%$; cysless = $103 \pm 1\%$ efflux maintained). The effect of $CdCl_2$ crosslinking reagent, however, was not as pronounced. The double-cysteine mutants maintained $68 \pm 5\%$ (K64C/V419C) and $89 \pm 2\%$ (K268C/W440C) of the original efflux after crosslinking with $CdCl_2$ (wild type = $90 \pm 1\%$; cysless = $104 \pm 6\%$). Example images of cells expressing $EAAC1_{K64C/V419C}$ and iGluSnFR before and after crosslinking with CuPh are shown in Fig. 6c. Before crosslinking, the cells showed a fluorescence increase of 43% with induction by K^+. After crosslinking, the same cells showed only a fluorescence increase of 3%, indicating that crosslinking reduced the glutamate efflux of these cells by about 94%.

No Effect of Crosslinking on Na^+ Binding to the Empty Transporter

It was previously shown that voltage jumps to the glutamate-free transporter result in Na^+-dependent transient charge movement [35, 36]. When applying step changes to the membrane potential for a period of 40 ms (voltage protocol shown in Fig. 7a, top), transient currents were observed, which were sensitive to 400 µM TBOA (used to correct for non-specific transient currents). In the absence of CuPh, these charge movements are shown in (Fig.7a–c). Results after crosslinking are shown in Fig. 7d–f. voltage jump-induced charge movements were preserved in both

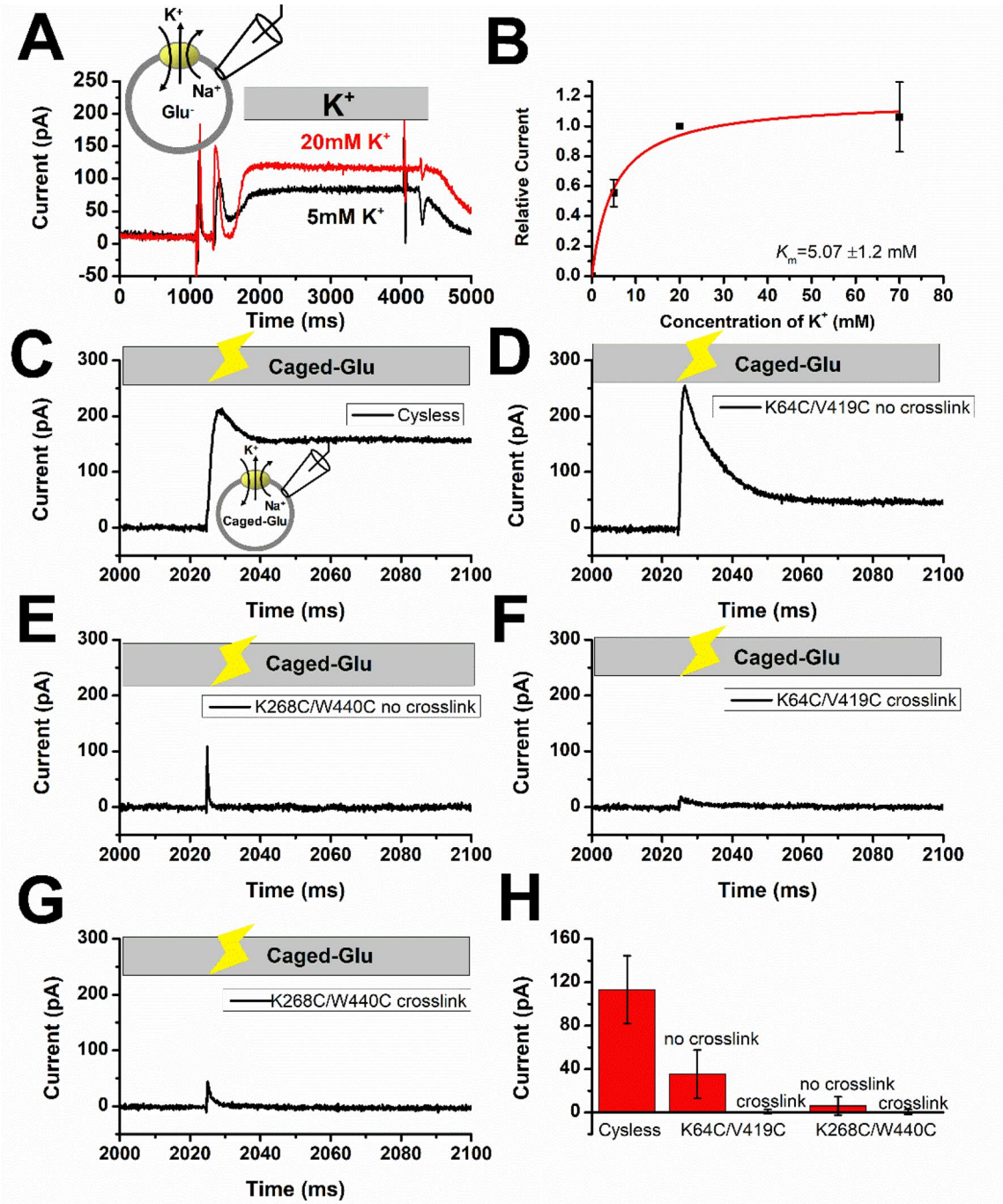

Fig. 5 Inhibition of reverse transport and charge movements by crosslinking. **a** Typical reverse transport currents of $EAAC1_{cysless}$ (in the absence of permeant anion) after application of extracellular K^+ (indicated by grey bar). The intracellular solution contained 130 mM NaMes and 5 mM glutamate. **b** Determination of K^+ apparent affinity from the dose response curve fitted with a Michaelis–Menten-like equation (red line). $EAAC1_{cysless}$ K_m for K^+ was 5.07 ± 1.2 mM. **c** Reverse transport laser photolysis experiment with $EAAC1_{cysless}$. The time of the laser pulse is indicated with the flash symbol. The extracellular solution contained 140 mM K^+, the intracellular solution contained 130 mM NaMES and 5 mM MNI-caged glutamate. **d** and **e** Similar experiment with $EAAC1_{K64C/V419C}$ (n = 35) and $EAAC1_{K268C/W440C}$ (n = 20) before crosslinking. **f** and **g** Laser photolysis experiment with $EAAC1_{K64C/V419C}$ (n = 12) and $EAAC1_{K268C/W440C}$ (n = 26) after crosslinking. **h** Comparison of steady-state reverse transport currents before and after crosslinking. The membrane potential was 0 mV in all experiments. Student's t-test results indicted the crosslink effect was significant for K268C/W440C, $p = 0.01$, and for K64C/V419C, $p < 0.000000001$

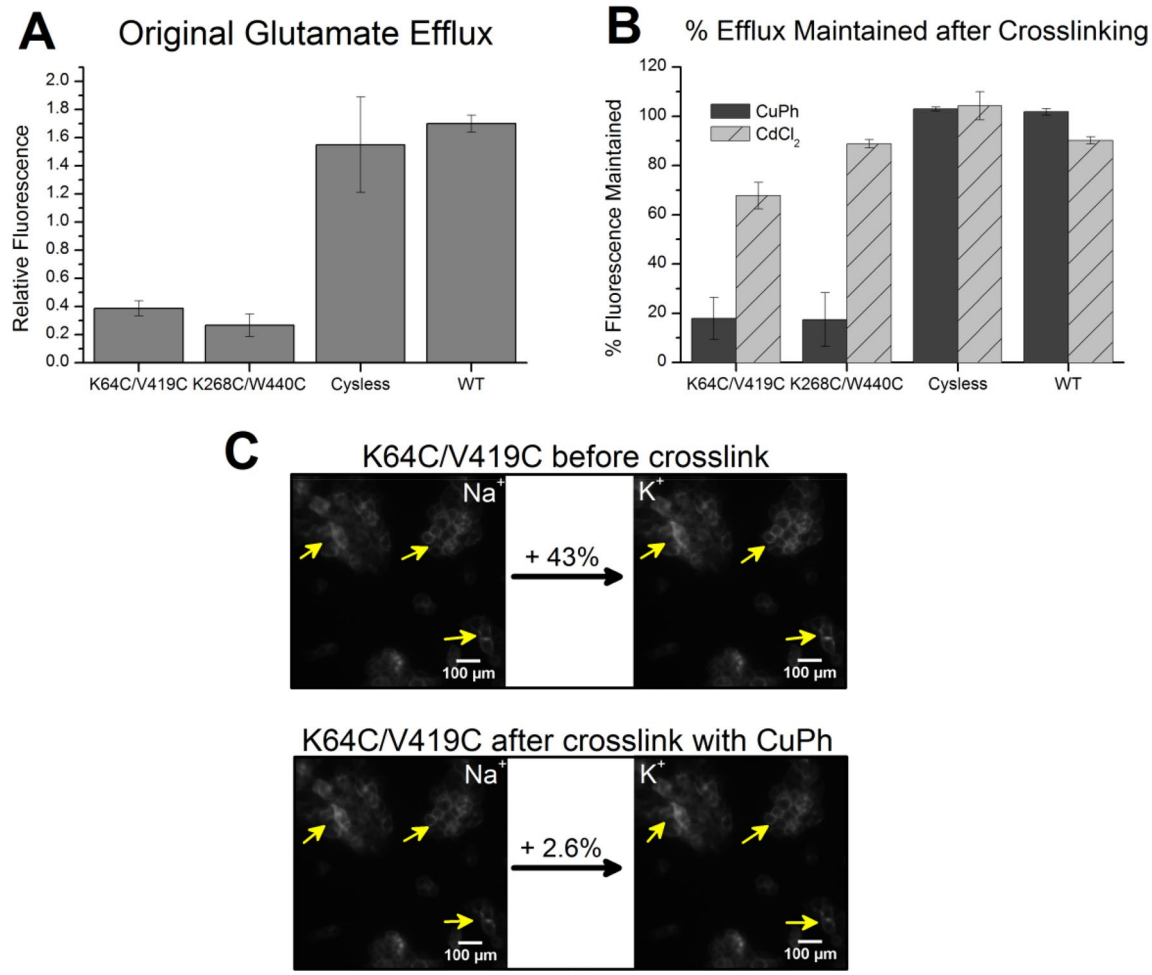

Fig. 6 K64C/V419C, K268C/W440C mutant transporters show significant decrease in glutamate efflux after crosslinking. iGluSnFr glutamate fluorescent sensor and EAAC1 transporter DNA (wild type, cysless, K64C/V419C or K268C/W440C) were co-expressed in HEK293 cells. **a** Relative glutamate efflux from cells (as measured by fluorescent sensor) induced by K^+ without the presence of crosslinking reagents (wild type = 1.70 ± 0.06 (n = 4); cysless = 1.55 ± 0.34 (n = 2); K64C/V419C = 0.39 ± 0.05 (n = 7); K268C/W440C = 0.27 ± 0.08 (n = 7)). Student's t-test analysis indicate significant difference compared to wild type for K64C/V419C $p < 0.00000001$ and K268C/W440C $p < 0.00000001$. **b** Percent of original fluorescence intensity maintained after crosslinking with CuPh (wild type = 102 ± 1% (n = 3); cysless = 103 ± 1% (n = 2); K64C/V419C = 18 ± 9% (n = 5); K268C/W440C = 17 ± 11% (n = 5)) and $CdC1_2$ (wild type = 90 ± 1% (n = 3); cysless = 104 ± 6% (n = 2); K64C/V419C = 68 ± 5% (n = 4); K268C/W440C = 89 ± 2% (n = 4)). T-test results indicate significant difference compared to wild type for K64C/V419C $p < 0.001$ and K268C/W440C $p < 0.001$ for CuPh and K64C/V419C $p < 0.05$ for $CdCl_2$. **c** Example images for the determination of glutamate efflux in $EAAC1_{K64C/V419C}$. The top panel shows one example of original efflux data for a selection of cells whereby the fluorescence intensity increased by 43% upon application of external K^+. After crosslinking with 400 µM CuPh (bottom panel), the efflux of these cells decreased to only a 2.6% change with application of K^+, which is an overall 94% decrease in efflux after crosslinking

K64C/V419C and K268C/W440C mutant transporters after crosslinking. We next integrated the transient current signal and plotted charge–voltage relationships, shown in Fig. 7c and f. The Q–V relationships were virtually unchanged by the crosslinks, suggesting that Na^+ binding and release steps in the glutamate-free transporter still function in the immobilized K64C/V419C and K268C/W440C mutant transporters. Control experiments in non-transfected cells are shown in Fig. 7g, demonstrating no charge movement.

Discussion

In this work, we extended crosslinking studies previously performed on glutamate transporters, to identify the effect of restricting conformational freedom of the transport domain on rapid kinetics and early reactions associated with the substrate transport process. We focused on crosslinking of two disulfide pairs, K268C/W440C, which was first generated by the Kanner group [25], and K64C/V419C, which was shown to stabilize the inward-facing conformation in Glt_{Ph} [20, 37].

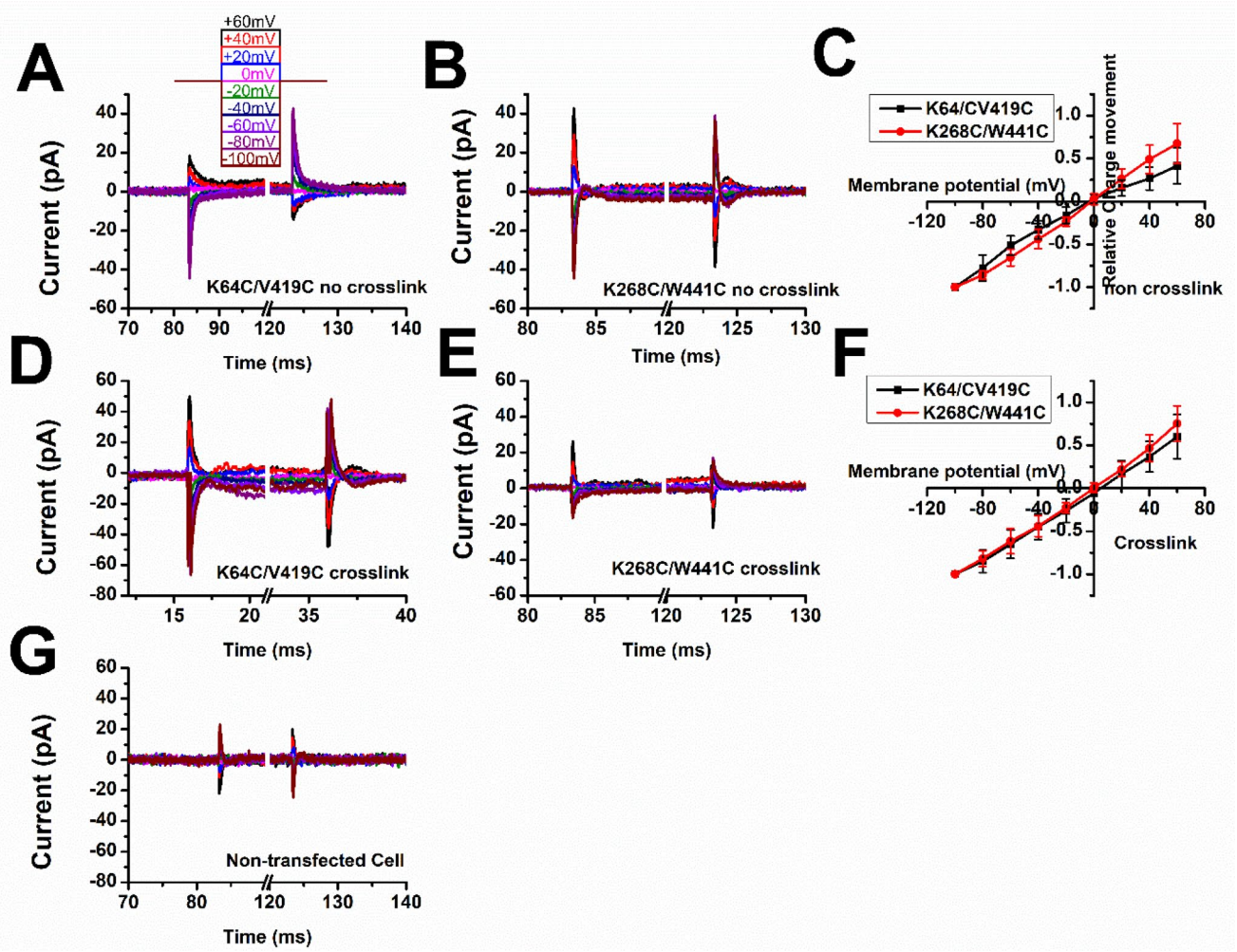

Fig. 7 Crosslinked transporters show transient current after voltage jumps in the absence of glutamate. A voltage-jump protocol shown in the inset of (A) was used to isolate Na^+-induced transient currents in the glutamate-free transporter in the absence of permeant anion. **a** and **b** Original transient current traces before crosslinking in K64C/V419C (n = 7) and K268C/W440C (n = 8) mutant transporters. Unspecific currents were subtracted using 400 µM TBOA. **d** and **e)** Similar experiments as in (A and B) but after crosslinking (n = 6 and 5). **c** and **f)** Charge movement as a function of the membrane potential obtained by integrating the transient current signals. The intracellular solution contained 130 mM KMes, the extracellular solution contained 140 mM NaMes. **g** Result of the same voltage jump experiment performed in non-transfected cells

Other cysteine pairs were also published to show successful crosslinking, based on EAAT1 and GLT-1. In these studies, EAAT1 [38–40] TM2-HP1, TM4-TM7 and TM4-TM8 were covalently linked, in addition to GLT-1 [41, 42] TM5-TM8, TM2-TM4 interactions. In these positions, double cysteine mutants showed significant crosslinking effects, with oxidizing conditions largely inhibiting the radiolabeled substrate uptake. In particular, a pair of cysteines highly sensitive to oxidation were identified in EAAT1 between TM4 and TM8, with low concentrations of CuPh at 600 nM leading to a complete inhibition effect [40].

In extension of previous studies, we applied the laser-photolysis method with caged glutamate, allowing the observation of early intermediates in the transport cycle by generating glutamate concentration jumps with a sub-millisecond time resolution. In wild-type and cysless glutamate transporters, charge movement in response to glutamate concentration jumps manifests itself in a pre-steady-state component that allows the differentiation of three phases, which can be separated on the time scale (Fig. 4a) [29]. These three phases were previously interpreted to be tightly associated with Na^+/Glu^- binding and translocation steps [29] (i.e. elevator-like movement of the transport domain relative to the membrane normal). The major result of the present study is that it is not only the steady-state transport that is blocked by the application of CuPh, consistent with previous publications, but that the pre-steady-state charge movement in the forward transport direction is also largely

inhibited (Fig. 4). This result may be expected for the K64C/V419C crosslink, which was proposed to lock the transporter in the inward-facing state [20]. Thus, forward translocation is unlikely to be possible after external application of glutamate. However, the K268C/W440C crosslink also prevented transient charge movement. While $EAAC1_{K268C/W440C}$ was much less active than the cysless transporter even before crosslinking, we attribute this effect to intrinsic crosslinking before CuPh application, as has been proposed in [25]. In any case, these results suggest that it is not only the translocation reaction itself, but also a conformational change associated glutamate-induced Na^+ binding, potentially the formation of the intermediate outward-facing state, that are blocked by the covalent restriction of TM8 relative to TM5.

In the reverse transport mode, both crosslinks virtually eliminated steady-state transport current, and significantly reduced glutamate release through reverse transport (Fig. 6). This result is expected because the immobilization of the transport domain most likely prevents the conformational changes necessary for glutamate release. In addition, very little pre-steady-state charge movement was observed in response to glutamate concentration jumps to the intracellular side of the membrane. For the K268C/W440C crosslink, this lack of charge movement is most likely caused by the inability of intracellular glutamate to bind to the transporter locked in the outward-facing conformation. However, for the K64C/V419C crosslink, the results are more interesting. It was previously shown by Boudker and colleagues that aspartate and Na^+ can bind to Glt_{Ph} with the analogous crosslink [20], which locks the transporter in the inward-facing configuration. This is consistent with the ability of glutamate transporter substrates to bind to brain membranes at low temperatures, when translocation is inhibited (i.e. an immobilized transport domain) [43]. If this is the case, the absence of glutamate-induced transient currents indicate that any of these binding reactions are almost electroneutral, or only weakly electrogenic. Our group had previously proposed that intracellular Na^+ binding to the empty transporter is electrogenic [27]. This intracellular Na^+ binding process could be responsible for the small, outwardly-directed charge movement that remains in the K64C/V419C crosslinked transporter (Fig. 5f). Overall, these reverse transport results suggest a strong inhibition of most early reaction steps in the reverse transport process in response to glutamate binding, including the reverse translocation step.

Interestingly, the glutamate-induced anion current was not fully abolished by oxidative crosslinking in the K268C/W440C mutant transporter (Fig. 2d). This result is consistent with a previous report by the Kanner group, suggesting that the crosslink still allows the anion-conducting state to be populated [25]. One possibility, which was already proposed by Kanner and colleagues [25] could be that the anion conductance is closely linked to the outward-facing intermediate state, which has been previously identified in structural studies [17]. This idea is consistent with proposals by the Fahlke group [11] that the anion conducting state is structurally similar, and in rapid equilibrium with the outward-facing intermediate state. This suggestion would also support previous rapid kinetic studies, in which the anion conducting state was placed along the translocation pathway [29]. While the distance between the two cysteine residues is larger in the intermediate state than in the outward-facing conformation (Fig. 1), it may still allow transient formation of this state, and, thus, anion conductance to function. In contrast, TBOA was unable to significantly block the leak anion conducting state after crosslinking the K268C/W440C mutant transporter (Fig. 2d). This suggests that the leak anion conducting state adopts a different structure than the glutamate-dependent anion conducting state. For the K64C/V419C crosslink, neither glutamate-induced anion conductance, nor TBOA-blockable leak anion conductance was observed (Fig. 2d), consistent with the idea that extracellularly-applied substrates or inhibitors cannot interact with the inward-facing configuration.

Finally, we tested for transient currents in response to voltage jumps in the empty, glutamate-free transporter (Fig. 7). It was previously proposed, by us and others [29, 44, 45], that these transient currents are caused by voltage-dependent Na^+ binding to the extracellular binding site. These transient currents can be isolated from non-specific current components by block with specific, competitive EAAT inhibitors, for example TBOA and kainate [44]. TBOA-sensitive transient currents were observed in crosslinked transporters with both K268C/W440C and K64C/V419C cysteine pairs (Fig. 7). For $EAAC1_{K268C/W440C}$, this results suggest that the Na^+ binding events to the empty transporter are still functional after crosslinking TM5 and TM8. Most likely, the electrogenic Na^+ binding reaction is not associated with major conformational changes of the transporter, or with structural changes that do not involve movement of TM5 relative to TM8. This conclusion is consistent with structural results from the *apo* and Na^+ bound Glt_{Tk} homologue. Here, major structural changes upon Na^+ binding were only observed in the unwound and highly-conserved NMDGT region of TM7, but not in the relative positioning between transport and trimerization domain [46]. For the transporter with the K64C/V419C crosslink, the results are more difficult to explain. If this crosslink results in an inward-facing state, it should be insensitive to extracellularly-applied TBOA. However, the TBOA-sensitive transient currents are substantial in size. One possibility is that, because of the high TBOA concentration used (about 1000 times K_m), the transporter inward-facing-outward-facing equilibrium can be pulled to the outward-facing state, despite the crosslink, although this would seemingly require a large distortion of the transporter structure (Fig. 1).

Conclusions

In this study, we tested K268C/W440C (between TM5 and TM8) and K64C/V419C (between TM2 and HP2) double-cysteine mutant transporters with respect to the effect of crosslinking on partial reactions in the transport cycle. From analysis of pre-steady-state currents in response to rapid glutamate concentration jumps in both forward and reverse transport mode, it was concluded that the crosslinks impair most pre-steady-state processes previously assigned to the glutamate translocation process, as well as Na^+-binding to the glutamate-bound form of the transporter, and conformational changes associated with it. Therefore, the crosslinks seem to severely restrain conformational flexibility of the transporter, which is necessary for these early reactions in the transport cycle to occur. In contrast, Na^+ binding to the glutamate-free form of the transporter, as well as to a minor extent the glutamate-induced anion conductance, were still operational, at least in the K268C/W440C mutant transporter. Overall, our results add to the previous mechanistic view of how covalent restraints of the transporter affect function and individual reaction steps in the transport cycle.

Experimental Section

Cell Culture and Transfection

HEK293 cells (American Type Culture Collection No. CRL 1573) were cultured as described previously [24]. Cell cultures were transiently transfected with wild-type or mutant EAAC1 cDNAs, inserted into a modified pBK-CMV-expression plasmid, using Jetprime transfection reagent according to the protocol supplied by the manufacturer (Polyplus). The cells were used for electrophysiological measurements between 24 and 36 h after transfection. The cysless EAAC1 variant contained Cys to Ser substitutions in positions 9, 158, 218, 255 and 342 and was generated using the QuikChange mutagenesis procedure (Agilent), followed by sequencing. K268C/W440C and K64C/V419C double-mutant transporter DNAs were generated within the $EAAC1_{cysless}$ background. The K268C/W440C transporter cDNA was a generous gift provided by Dr. Baruch Kanner. K64C/V419C mutations were generated by Gene Universal Co. Ltd.

Crosslinking Procedures

The solutions of CuPh (Copper 1,10-Phenanthroline) and $CdCl_2$ were prepared as 10 mM stock solutions in NMG-MES (NMG: N-Methylglucaminegluconate, MES: Methanesulfonate) solution and diluted to 400 µM concentration with external buffer solution (see below) prior to each experiment. DTT (Dithiothreitol) was prepared as a 20 mM stock solutions in NMG-MES solution. Cells were incubated in crosslink or protective solutions at room temperature for 15 min before electrophysiology experiments were started.

Solution Exchange and Laser Photolysis

Rapid solution exchange (time resolution 100–200 ms) was performed by means of a quartz tube (opening diameter 350 µm) positioned at a distance of 0.5 mm to the cell. The linear flow rate of the solutions emerging from the opening of the tube was 5–10 cm/s. Laser-pulse photolysis experiments were performed as described in detail previously [47]. In the reverse transport experiments, MNI-caged glutamate were introduced into the cell through the glass recording electrode. After whole-cell mode was established, a period of 5 mins was allowed for diffusive equilibration with the cell interior. MNI-caged glutamate [48, 49], at concentrations of 1 mM (140 mM and 49 mM Na^+) to 4 mM (18 mM and 10 mM Na^+), or free glutamate were applied to the cells and photolysis of the caged glutamate was initiated with a light flash (355 nm, 8 ns, Minlite II, Continuum). The light was coupled into a quartz fiber (diameter 365 µm) that was positioned in front of the cell in a distance of 300 µm. With maximum light intensities of 500–840 mJ/cm^2 saturating glutamate concentrations could be released, which was tested by comparison of the steady-state current with that generated by rapid perfusion of the same cell with 1 mM caged glutamate with 140 mM Na^+. Data were recorded using the pClamp6 software (Axon Instruments), digitized with a sampling rate of 1 kHz (solution exchange) or 25 kHz (laser photolysis and voltage jump) and low-pass filtered at 250 Hz or 3–10 kHz, respectively.

Electrophysiology

Currents associated with glutamate transporters were measured in the whole-cell current recording configuration. Whole-cell currents were recorded with an EPC7 patch-clamp Amplifier (ALA Scientific, Westbury, NY) under voltage-clamp conditions. The resistance of the recording electrode was 3–6 MΩ. Series resistance was not compensated because of the relatively small whole-cell currents carried by EAAC1, in both anion and transport modes. The composition of the solutions for measuring transport currents or laser-photolysis experiments was: 140 mM NaMes, 2 mM $MgGluconate_2$, 2 mM $CaMes_2$, 10 mM 4-(2-Hydroxyethyl) piperazine-1-ethanesulfonic acid (HEPES), 10 mM glutamate, pH 7.3 (extracellular), 130 mM KMes (Mes = methanesulfonate), 2 mM $MgGluconate_2$, 5 mM Ethylene glycol-bis(2-aminoethylether)-*N*,*N*,*N*',*N*'-tetraacetic acid (EGTA),

10 mM HEPES, pH 7.3 (intracellular). For anion current recordings, intracellular Mes was replaced by SCN^-. For reverse transport current recordings, KMes was used as external solution, 130 mM NaMes and 5 mM Glutamate as internal solution, as published previously [24, 30, 32].

Voltage Jumps

Voltage jumps (-100 to + 60 mV) were applied to perturb the electrogenic glutamate translocation equilibrium. To determine EAAC1-specific currents, control currents were recorded in the presence of 400 µM extracellular TBOA (DL-threo-β-benzyloxyaspartic acid) and subtracted from the glutamate-induced currents. Capacitive transient compensation and series resistance compensation of up to 80% was employed using the EPC-7 amplifier. Non-specific transient currents were subtracted in Clampfit software (Molecular Devices).

Cellular Glutamate Efflux Measured by Extracellular Glutamate-Binding Sensor

EAAC1 transporter was co-expressed with iGluSnFR [34, 50] extracellular glutamate-binding sensor in HEK293 cells as a system for measuring glutamate efflux via fluorescence intensity changes. The sensor is bound to the outside of the cell membrane and contains a glutamate-binding component that responds rapidly to extracellular glutamate concentration changes. The external glutamate concentration is reported via fluorescent intensity change. This method specifically isolates the transport function of EAAC1 in response to various external conditions and eliminates the variable of anion conductance.

Imaging experiments were performed as described previously [50]. All imaging experiments utilized a live-cell flow-through imaging chamber (Warner Instruments, Series 20) together with an inverted fluorescence microscope (Zeiss Axiovert 25). The fluorescence filter set used was FITC, which was obtained from Omega Filters. Bath buffer solution contained NaMes (Mes = methanesulfonate) and KMes equaling a combined concentration of 140 mM, 2 mM $CaGluconate_2$, 2 mM $MgGluconate_2$, 10 mM 4-(2-Hydroxyethyl) piperazine-1- ethanesulfonic acid (HEPES), pH 7.3 using NaOH. 140 mM NaMes solution was used to initially wash the remaining culturing medium from the cell surface and also in between each test solution to act as a benchmark for changes in fluorescence. Solutions were passed through the imaging chamber for 30–45 s before recording an image. For each experiment, the exposure and other imaging features were set as constant and for an appropriate fluorescence intensity below saturation. Images were recorded after each solution exchange and then analyzed using ImageJ software [51]. ImageJ was used to quantify the fluorescence intensity of 5–10 cells per image. The loci were held constant when comparing images in an experiment. The relative fluorescence change (ΔF/F) was calculated as follows:

$$\frac{\Delta F}{F} = \frac{F_{\text{final}} - F_{\text{initial}}}{F_{\text{initial}}} \quad (1)$$

where F_{initial} was the fluorescence intensity of the image taken after passing the initial solution directly prior to the test solution, and F_{final} was the fluorescence intensity of the same point in the image taken following the test solution.

Data Analysis

All data are shown as mean ± SD, collected from recordings of 8 to 10 cells. For statistical analysis, paired two-tailed *t* tests were used in Microsoft Excel software. To determine K_m values, non-linear curve fitting was used with a Michaelis–Menten-like equation, $y = I_{max} * [Glu]/(K_m + [Glu])$ built in the Origin software least-squares-fitting package. Mean values were compared by using two tailed student's t-test results. These results were calculated using Microsoft Excel.

Nonlinear regression fits of laser-pulse photolysis experimental results were performed in Clampfit software (Axon Instruments) by the use of the following equations. The pre-steady-state transport currents and (in the absence of SCN) were fitted with a sum of three exponential functions and a stationary current component: $I = I_1 \cdot \exp(-t/\tau_{rise}) + I_2 \cdot \exp(-t/\tau_{decay1}) + I_3 \cdot \exp(-t/\tau_{decay2}) + I_{SS}$. Here, I is the current amplitude, τ the time constant, and t the time.

Supplementary Information The online version of this article (https://doi.org/10.1007/s11064-021-03247-8) contains supplementary material, which is available to authorized users.

Acknowledgements This work was supported by a National Institutes of Health (NIH), Grant 1 R15 GM135843-01 awarded to CG.

References

1. Zerangue N, Kavanaugh MP (1996) Flux coupling in a neuronal glutamate transporter. Nature 383:634–637
2. Tanaka K, Watase K, Manabe T, Yamada K, Watanabe M, Takahashi K, Iwama H, Nishikawa T, Ichihara N, Kikuchi T, Okuyama S, Kawashima N, Hori S, Takimoto M, Wada K (1997) Epilepsy and exacerbation of brain injury in mice lacking the glutamate transporter GLT-1. Science 276:1699–1702
3. Pines G, Kanner BI (1990) Counterflow of L-glutamate in plasma membrane vesicles and reconstituted preparations from rat brain. Biochemistry 29:11209–11214
4. Wadiche JI, Amara SG, Kavanaugh MP (1995) Ion fluxes associated with excitatory amino acid transport. Neuron 15:721–728
5. Kanner BI, Sharon I (1978) Active transport of L-glutamate by membrane vesicles isolated from rat brain. Biochemistry 17:3949–3953

6. Kavanaugh MP, Bendahan A, Zerangue N, Zhang Y, Kanner BI (1997) Mutation of an amino acid residue influencing potassium coupling in the glutamate transporter GLT-1 induces obligate exchange. J Biol Chem 272:1703–1708
7. Zhang Y, Bendahan A, Zarbiv R, Kavanaugh MP, Kanner BI (1998) Molecular determinant of ion selectivity of a (Na+ + K+)-coupled rat brain glutamate transporter. Proc Natl Acad Sci U S A 95:751–755
8. Zerangue N, Kavanaugh MP (1996) Interaction of L-cysteine with a human excitatory amino acid transporter. J Physiol 493(Pt 2):419–423
9. Levy LM, Warr O, Attwell D (1998) Stoichiometry of the glial glutamate transporter GLT-1 expressed inducibly in a Chinese hamster ovary cell line selected for low endogenous Na+-dependent glutamate uptake. J Neurosci 18:9620–9628
10. Bergles DE, Tzingounis AV, Jahr CE (2002) Comparison of coupled and uncoupled currents during glutamate uptake by GLT-1 transporters. J Neurosci 22:10153–10162
11. Machtens JP, Kortzak D, Lansche C, Leinenweber A, Kilian P, Begemann B, Zachariae U, Ewers D, de Groot BL, Briones R, Fahlke C (2015) Mechanisms of anion conduction by coupled glutamate transporters. Cell 160:542–553
12. Fairman WA, Vandenberg RJ, Arriza JL, Kavanaugh MP, Amara SG (1995) An excitatory amino-acid transporter with properties of a ligand-gated chloride channel. Nature 375:599–603
13. Arriza JL, Eliasof S, Kavanaugh MP, Amara SG (1997) Excitatory amino acid transporter 5, a retinal glutamate transporter coupled to a chloride conductance. Proc Natl Acad Sci U S A 94:4155–4160
14. Leary GP, Stone EF, Holley DC, Kavanaugh MP (2007) The glutamate and chloride permeation pathways are colocalized in individual neuronal glutamate transporter subunits. J Neurosci 27:2938–2942
15. Yernool D, Boudker O, Jin Y, Gouaux E (2004) Structure of a glutamate transporter homologue from Pyrococcus horikoshii. Nature 431:811–818
16. Grewer C, Balani P, Weidenfeller C, Bartusel T, Tao Z, Rauen T (2005) Individual subunits of the glutamate transporter EAAC1 homotrimer function independently of each other. Biochemistry 44:11913–11923
17. Verdon G, Boudker O (2012) Crystal structure of an asymmetric trimer of a bacterial glutamate transporter homolog. Nat Struct Mol Biol 19:355–357
18. Koch HP, Brown RL, Larsson HP (2007) The glutamate-activated anion conductance in excitatory amino acid transporters is gated independently by the individual subunits. J Neurosci 27:2943–2947
19. Boudker O, Ryan RM, Yernool D, Shimamoto K, Gouaux E (2007) Coupling substrate and ion binding to extracellular gate of a sodium-dependent aspartate transporter. Nature 445:387–393
20. Reyes N, Ginter C, Boudker O (2009) Transport mechanism of a bacterial homologue of glutamate transporters. Nature 462:880–885
21. Crisman TJ, Qu S, Kanner BI, Forrest LR (2009) Inward-facing conformation of glutamate transporters as revealed by their inverted-topology structural repeats. Proc Natl Acad Sci U S A 106:20752–20757
22. Bendahan A, Armon A, Madani N, Kavanaugh MP, Kanner BI (2000) Arginine 447 plays a pivotal role in substrate interactions in a neuronal glutamate transporter. J Biol Chem 275:37436–37442
23. Kanner BI, Bendahan A (1982) Binding order of substrates to the sodium and potassium ion coupled L-glutamic acid transporter from rat brain. Biochemistry 21:6327–6330
24. Wang J, Albers T, Grewer C (2018) Energy Landscape of the Substrate Translocation Equilibrium of Plasma-Membrane Glutamate Transporters. J Phys Chem B 122:28–39
25. Shabaneh M, Rosental N, Kanner BI (2014) Disulfide cross-linking of transport and trimerization domains of a neuronal glutamate transporter restricts the role of the substrate to the gating of the anion conductance. J Biol Chem 289:11175–11182
26. Grewer C, Watzke N, Wiessner M, Rauen T (2000) Glutamate translocation of the neuronal glutamate transporter EAAC1 occurs within milliseconds. Proc Natl Acad Sci U S A 97:9706–9711
27. Zhang Z, Tao Z, Gameiro A, Barcelona S, Braams S, Rauen T, Grewer C (2007) Transport direction determines the kinetics of substrate transport by the glutamate transporter EAAC1. Proc Natl Acad Sci U S A 104:18025–18030
28. Wadiche JI, Kavanaugh MP (1998) Macroscopic and microscopic properties of a cloned glutamate transporter/chloride channel. J Neurosci 18:7650–7661
29. Watzke N, Bamberg E, Grewer C (2001) Early intermediates in the transport cycle of the neuronal excitatory amino acid carrier EAAC1. J Gen Physiol 117:547–562
30. Wang J, Zielewicz L, Grewer C (2019) A K(+)/Na(+) co-binding state: Simultaneous versus competitive binding of K(+) and Na(+) to glutamate transporters. J Biol Chem
31. Otis TS, Jahr CE (1998) Anion currents and predicted glutamate flux through a neuronal glutamate transporter. J Neurosci 18:7099–7110
32. Wang J, Zhang K, Goyal P, Grewer C (2020) Mechanism and potential sites of potassium interaction with glutamate transporters. J Gen Physiol 152
33. Szatkowski M, Barbour B, Attwell D (1990) Non-vesicular release of glutamate from glial cells by reversed electrogenic glutamate uptake. Nature 348:443–446
34. Marvin JS, Borghuis BG, Tian L, Cichon J, Harnett MT, Akerboom J, Gordus A, Renninger SL, Chen TW, Bargmann CI, Orger MB, Schreiter ER, Demb JB, Gan WB, Hires SA, Looger LL (2013) An optimized fluorescent probe for visualizing glutamate neurotransmission. Nat Methods 10:162–170
35. Grewer C, Zhang Z, Mwaura J, Albers T, Schwartz A, Gameiro A (2012) Charge compensation mechanism of a Na+-coupled, secondary active glutamate transporter. J Biol Chem 287:26921–26931
36. Wadiche JI, Arriza JL, Amara SG, Kavanaugh MP (1995) Kinetics of a human glutamate transporter. Neuron 14:1019–1027
37. Ryan RM, Mitrovic AD, Vandenberg RJ (2004) The chloride permeation pathway of a glutamate transporter and its proximity to the glutamate translocation pathway. J Biol Chem 279:20742–20751
38. Zhang W, Zhang X, Qu S (2019) Substrate-Induced Motion between TM4 and TM7 of the Glutamate Transporter EAAT1 Revealed by Paired Cysteine Mutagenesis. Mol Pharmacol 95:33–42
39. Zhang Y, Zhang X, Qu S (2014) Cysteine mutagenesis reveals alternate proximity between transmembrane domain 2 and hairpin loop 1 of the glutamate transporter EAAT1. Amino Acids 46:1697–1705
40. Qu S, Zhang W, He S, Zhang X (2019) Paired-Cysteine Scanning Reveals Conformationally Sensitive Proximity between the TM4b-4c Loop and TM8 of the Glutamate Transporter EAAT1. ACS Chem Neurosci 10:2541–2550
41. Rong X, Tan F, Wu X, Zhang X, Lu L, Zou X, Qu S (2016) TM4 of the glutamate transporter GLT-1 experiences substrate-induced motion during the transport cycle. Sci Rep 6:34522
42. Zhang X, Qu S (2011) Proximity of transmembrane segments 5 and 8 of the glutamate transporter GLT-1 inferred from paired cysteine mutagenesis. PLoS One 6:e21288

43. Aprico K, Beart PM, Crawford D, O'Shea RD (2004) Binding and transport of [3H](2S,4R)- 4-methylglutamate, a new ligand for glutamate transporters, demonstrate labeling of EAAT1 in cultured murine astrocytes. J Neurosci Res 75:751–759
44. Zielewicz L, Wang J, Ndaru E, Grewer CT (2019) Transient Kinetics Reveal Mechanism and Voltage Dependence of Inhibitor and Substrate Binding to Glutamate Transporters. ACS Chem Biol
45. Mennerick S, Shen W, Xu W, Benz A, Tanaka K, Shimamoto K, Isenberg KE, Krause JE, Zorumski CF (1999) Substrate turnover by transporters curtails synaptic glutamate transients. J Neurosci 19:9242–9251
46. Guskov A, Jensen S, Faustino I, Marrink SJ, Slotboom DJ (2016) Coupled binding mechanism of three sodium ions and aspartate in the glutamate transporter homologue GltTk. Nat Commun 7:13420
47. Niu L, Wieboldt R, Ramesh D, Carpenter BK, Hess GP (1996) Synthesis and characterization of a caged receptor ligand suitable for chemical kinetic investigations of the glycine receptor in the 3-microseconds time domain. Biochemistry 35:8136–8142
48. Canepari M, Nelson L, Papageorgiou G, Corrie JE, Ogden D (2001) Photochemical and pharmacological evaluation of 7-nitroindolinyl-and 4-methoxy-7-nitroindolinyl-amino acids as novel, fast caged neurotransmitters. J Neurosci Methods 112:29–42
49. Wieboldt R, Gee KR, Niu L, Ramesh D, Carpenter BK, Hess GP (1994) Photolabile precursors of glutamate: synthesis, photochemical properties, and activation of glutamate receptors on a microsecond time scale. Proc Natl Acad Sci U S A 91:8752–8756
50. Zielewicz L, Grewer C (2019) Genetically Encoded Halide Sensor-Based Fluorescent Assay for Rapid Screening of Glutamate Transport and Inhibition. ACS Sens 4:2358–2366
51. Arena ET, Rueden CT, Hiner MC, Wang S, Yuan M, Eliceiri KW (2017) Quantitating the cell: turning images into numbers with ImageJ. Wiley Interdiscip Rev Dev Biol 6